ELSEVIER

Engineering Analysis with Boundary Elements ▮ (▮▮▮▮) ▮▮▮–▮▮▮

ENGINEERING ANALYSIS with BOUNDARY ELEMENTS

www.elsevier.com/locate/enganabound

Infinite boundary elements in 2D elasticity

Alberto Salvadori

DICATA, University of Brescia, via Branze 38, 25123 Brescia, Italy

Received 5 February 2007; accepted 16 June 2007

Abstract

In the present note, three infinite boundary elements are proposed for the quasi-static 2D elastic problem. Within the framework of hypersingular boundary integral equations, a polynomial decaying, a reciprocal decaying, and a constant-logarithmic infinite boundary element are formulated, implemented and tested with respect to the analytical 2D plane strain solution of a strip load on a half-plane.

Keywords: Unbounded domains; Infinite boundary elements; Boussinesque problem

1. Introduction

Modeling unbounded domains is an important issue in engineering: electro-magnetism, fluid dynamics, soil and soil-structure mechanics are but a few areas in which unbounded domains are of usual concern [1–3]. The present work focuses on the last topic and shall be conceived as a first step towards modeling half-plane engineering problems—as foundation vibration problems—in the frequency domain.

Whereas in studying the dynamics of soils it is important to take into account their porous nature [4], in soil-structure interaction problems a one-phase linearized modeling of the ground can often be accepted. The unbounded nature of the domain can be reproduced in two ways: (i) by selecting a fictitious truncated domain; (ii) via *infinite domain techniques*, the topic the present note deals with. In the first class, the so-called *finite domain technique*, the most challenging task—especially in dynamics [5]—is enforcing the appropriate boundary conditions along the artificial boundaries that give rise from the domain truncation: the bibliography on this important topic is extremely large.

In all *infinite domain techniques* the problem domain remains unbounded. The numerical solution can be achieved by several methods: in the finite element method (FEM), the use of suitable infinite elements is required;[1] in the boundary element method (BEM), the fundamental solutions for a half-space [7] can be considered to solve the problem along the boundary. Such an approach reveals to be quite time consuming,[2] due to the complexity of the involved kernels. To avoid such a drawback, infinite elements have been implemented in the framework of the BEM as well[3] adopting the fullspace solution (Kelvin–Gebbia solution in statics, Stokes solution for frequency-domain problems).

Following [13], infinite elements can be categorized into two types, namely *displacement descent* or *elements with*

[1]Indeed many commercial codes do implement infinite elements for half-plane problems, see among others [6].

[2]If the half-space fundamental solution is used (Mindlin solution for static problems, Lamb solution for frequency-domain problems) there is no need for infinite boundary elements. Moreover, only the loaded surface, and in case other finite surfaces like tunnel openings, need to be discretized. Thus there is the advantage of having less unknowns and the disadvantage of a more involved calculation, that implies higher CPU times, even by a factor of 300 [8]. Half-space fundamental solutions were used for instance to formulate the axisymmetric BIE for a layered viscoelastic half-space [9,10]. In [11] two strategies are used alternatively: at the internal points, infinite elements permit using the fundamental solutions for a full-space to evaluate strains and stresses, thus decreasing the elaboration time.

[3]Accordingly, a truncation problem arises. However, truncation with BE has less consequences than truncation with FE: FE truncation implies the whole domain and not merely its surface. BEM relying on Stokes solution with truncated meshes were successfully used in soil-structure problems [12].

E-mail address: alberto@ing.unibs.it

0955-7997/$ - see front matter
doi:10.1016/j.enganabound.2007.06.007

Please cite this article as: Salvadori A. Infinite boundary elements in 2D elasticity. Eng Anal Bound Elem (2007), doi:10.1016/j.enganabound.2007.06.007

decaying functions [14–16] and *co-ordinate ascent* or *elements of the mapped kind* [17,18]. In the displacement descent formulation, the domain of natural co-ordinate is assumed to be extending to infinity. The field variable shape functions are obtained by modifying the usual shape functions to a descent towards infinity. This is achieved by incorporating a decay pattern into the conventional shape functions of the C^0 type. On the other hand, in the case of co-ordinate ascent formulation, the domain of natural co-ordinate is assumed to be finite. Ascent shape functions are used with a singularity at the boundary nodes, which sends the physical co-ordinates to infinity, whereas the conventional shape functions for the C^0 type are used in the field variables transformation. By comparing the above two formulations with each other, it can be found that the displacement descent formulation requires numerical integration over a semi-infinite range, whereas for the co-ordinate ascent formulation, integration can be made using the conventional Gauss–Legendre integration scheme. The success of formulation of any infinite element is contingent on satisfying some requirements [13]: in particular the shape function behavior at infinity should reproduce the asymptotic behavior of the problem solution.

In the context of linear elasticity, a reciprocal—with respect to the distance from a reference point—decaying shape function was proposed in [19] in order to model the unknown displacement field along the boundary. Such a formulation was further developed in [20] by defining a mapped infinite element onto the unit square. In [21] efficient criteria for numerical integration over unbounded domains have been applied to the aforementioned infinite element. The algorithm was further improved in a subsequent paper [22] by means of the analytical integration of the strongly singular elasticity kernel.

All aforementioned works have two distinct peculiarities. They: (i) deal with infinite boundary elements for 3D problems; (ii) lie in the framework of the collocation scheme.

About the first point, it might be seen as "a consequence of the impossibility of having truly 2D unbounded problem domains" (taken from [3, p. 40]). Nevertheless, many 2D problems have well-known closed form solutions (see e.g. [23]); moreover, 2D numerical simulations are of usual concern for engineering problems with unbounded domains. To this aim, 2D infinite elements have been widely proposed in the framework of linear elastic problems: a deep review, up to 1992, can be found in [3]. In 2D problems "it is easy to see that in general stresses vary as $1/r$ and thus so will strains. On integration the displacement field will have a logarithmic form. Since $\log r$ increases with r this gives the paradoxical result that the displacements at an infinite radius will, themselves, be infinite." (taken from [3, p. 13]). Such a paradox led to seek infinite elements with displacement approximation behavior of the form $1/r$ even in 2D problems, starting from the pioneering works up to the most recent ones [13,24–28]—about FEM as well as about BEM; infinite elements with reciprocal decaying shape functions are currently implemented in many commercial codes [6]. An insight on the asymptotical behavior of the displacement field is provided in Section 4.1: by comparing the half-plane solution and the asymptotic behavior of a half-space solution, an attempt is made to give a rationale to the use of reciprocal decaying shape functions to model the displacement field at infinity. A boundary infinite element is thereafter proposed and implemented by means of analytical integrations.

On the other hand, "It might be possible to devise an infinite element which incorporated a logarithmic behavior. This has not yet been tried." (taken from [3, p. 42]). In Section 5 an infinite element with constant and logarithmic shape functions is proposed—which to the best of our knowledge, has not been considered so far—and once again implemented by means of analytical and numerical integration schemes.

As a second characteristic of all cited works, numerical analysis refer to the boundary element collocation method. As a main consequence, the Somigliana identity is invoked in the solution process on the boundary, thus merely involving strong singularities in the formulation. The symmetric Galerkin boundary element (SGBEM) scheme [29], makes use of the boundary integral representation (BIR) of tractions, that involves a hypersingular Green's function (here collected in matrix $\mathbf{G}_{pp}$). The problem of hypersingular kernel integrations over finite domains has been overcome in the last two decades by several authors with different techniques: with reference to analytical integrations in two dimensions, the problem has been investigated in Ref. [30] without the recourse to regularization techniques. On the contrary, the problem of singular and hypersingular kernel integrations over unbounded domains apparently requires further study for the Galerkin scheme: to this topic a further publication will be devoted shortly.

In the present note, three boundary infinite elements are proposed and implemented: one of them in the hypersingular collocation framework, the remaining in the SGBEM as well. Apparently, unsurmountable difficulties come into play in the formulation of an SGBEM scheme for general shape functions on 2D unbounded elements. Such difficulties are rooted in the variational formulation of the elastic problem in 2D half-plane, because the total potential energy of the solution of the elastic problem is itself unbounded. From the computational side, this fact led to using weighted functional spaces that give rise to the Petrov–Galerkin method. A further publication will be devoted to the afore sketched issues. In the present, three different elements have been proposed: a *polynomial decaying element*, where the displacement field is approximated by high order lagrangian polynomials truncated "suitably" far away from the loaded zone; a *reciprocal* $1/r$ *decaying element*, analogous to [15]; a *constant and logarithmic decaying element*. In all three cases, analytical integrations for the hypersingular kernel have been

Please cite this article as: Salvadori A. Infinite boundary elements in 2D elasticity. Eng Anal Bound Elem (2007), doi:10.1016/j.enganabound.2007.06.007

produced.[4] The polynomial decaying element has a usual finite domain: accordingly, making use of analytical integrations that apply to standard polynomial boundary elements [30] is allowable. For the *reciprocal* $1/r$ *decaying element* analytical integrations have been performed in Section 4 in the general case. For the *constant and logarithmic decaying element* analytical integrations have been performed in Section 5 in the easy case of field point collinear or inside the unbounded element, whereas for the general case suitable numerical schemes [31] are considered.

The proposed elements have been compared in a benchmark application—Section 6—in terms of accuracy. The constant logarithmic element shown to be the most accurate and effective.

2. Boundary integral equations in elasticity

2.1. Single-zone formulation

Consider a homogeneous isotropic linear elastic solid in a Cartesian reference system, with unbounded domain $\Omega \subset \mathbb{R}^2$ and with an unbounded Neumann boundary Γ_p: assuming small strains and displacements, consider its response to quasi-static external tractions $\bar{\mathbf{t}}(\mathbf{x})$ on Γ_p (see the prototype of Fig. 3).

The boundary integral formulation of a linear elastic problem stems from Somigliana's identity, which is the BIR of displacements in the interior of domain Ω. Somigliana's identity is based on Green's functions (also called kernels) which represent components u_i of the displacement vector $\mathbf{u}$ in a point $\mathbf{x}$ due to: (i) a unit force concentrated in space (point $\mathbf{y}$) and acting on the unbounded elastic space Ω_∞ in direction j (such functions are gathered in matrix $\mathbf{G}_{uu}(\mathbf{x}-\mathbf{y})$); (ii) a unit relative displacement concentrated in space (at a point $\mathbf{y}$), crossing a surface with normal $\mathbf{l}(\mathbf{y})$ and acting on the unbounded elastic space Ω_∞ (in direction j) (gathered in matrix $\mathbf{G}_{up}(\mathbf{x}-\mathbf{y})$).

Because all the above introduced kernels are infinitely smooth in their domain, which is the whole space $\mathbb{R}^2$ with exception of the origin (that is $\mathbf{x} \neq \mathbf{y}$), the traction operator can be applied to Somigliana's identity, thus obtaining the BIR of tractions on a surface of normal $\mathbf{n}(\mathbf{x})$ in the interior of the domain. Such a BIR, by some authors named "hypersingular identity", involves Green's functions (collected in matrices $\mathbf{G}_{pu}$ and $\mathbf{G}_{pp}$) which describe components (p_i) of the traction vector $\mathbf{p}$ on a surface of normal $\mathbf{n}(\mathbf{x})$ due to: (i) a unit force concentrated in space (point $\mathbf{y}$) and acting on the unbounded elastic space Ω_∞ in direction j; (ii) a unit relative displacement concentrated in space (at a point $\mathbf{y}$), crossing a surface with normal $\mathbf{l}(\mathbf{y})$ and acting on the unbounded elastic space Ω_∞ (in direction j).

[4]Analytical integrations in the framework of unbounded boundary elements are not uncommon [22], because they obviate the need of performing numerical integrations on unbounded regions.

BIEs for the linear elastic problem can be derived from the aforementioned two representation formulae performing the boundary limit[5] $\Omega \ni \mathbf{x} \to \mathbf{x}^o \in \Gamma$. In the limit process: (i) singularities of Green's functions are triggered off: kernel $\mathbf{G}_{pu}$ presents a strong singularity of $O(r^{-2})$, whereas kernel $\mathbf{G}_{pp}$ is usually named hypersingular, since it shows a singularity of $O(r^{-3})$ greater than the dimension of the integral; (ii) strongly singular kernel $\mathbf{G}_{pu}$ generates a free term that holds $\frac{1}{2}$ for smooth boundaries; (iii) the following BIE comes out [33]:

$$\frac{1}{2}\mathbf{p}(\mathbf{x}) + \neq\!\!\!\!\!\int_{\Gamma_p} \mathbf{G}_{pp}(\mathbf{r};\mathbf{n}(\mathbf{x});\mathbf{l}(\mathbf{y}))\mathbf{u}(\mathbf{y})\,\mathrm{d}\mathbf{y} = \int_{\Gamma_p} \mathbf{G}_{pu}(\mathbf{r};\mathbf{n}(\mathbf{x}))\bar{\mathbf{p}}(\mathbf{y})\,\mathrm{d}\mathbf{y}, \quad \mathbf{x} \in \Gamma_p \tag{1}$$

having set $\mathbf{r} = \mathbf{x} - \mathbf{y}$. After imposing the fulfillment of Eq. (1) on Γ_p, one obtains a linear boundary integral problem

$$\mathscr{M}u = p \tag{2}$$

whose operator $\mathscr{M}$ is symmetric with respect to a classical bilinear form. Accordingly, the problem admits of a variational formulation and its solution is shown to be a maximum—on a suitable functional space V—of the functional:

$$\Psi[u] = \tfrac{1}{2}\mathscr{A}(u, \mathscr{M}u) - \mathscr{A}(u, p). \tag{3}$$

Rather unexpectedly, classical solution of elasticity—as Boussinesques' ones—do not belong to V, what seems to state that energy implications of functional (3) have not been sufficiently investigated on unbounded domains. Some remarks on this issue are presented in Section 4.1, whereas for details the reader is referred to a forthcoming publication.

2.2. Symmetric Galerkin approximation

Let $h > 0$ be a parameter and let U_h denote a family of finite dimensional subspaces of U such that

$$\forall \dot{u} \in U, \inf_{\dot{u}_h \in U_h} \|\dot{u} - \dot{u}_h\| \to 0 \quad \text{as } h \to 0. \tag{4}$$

The symmetric Galerkin approximation of (2) consists in finding $\dot{u}_h \in U_h$ critical point of the functional

$$\Psi[\dot{u}_h] = \tfrac{1}{2}\mathscr{A}(\dot{u}_h, \mathscr{M}\dot{u}_h) - \mathscr{A}(\dot{u}_h, \dot{p}). \tag{5}$$

From the algebraic point of view, let $\boldsymbol{\psi}_u(\mathbf{y})$ be a matrix of shape functions and $\mathbf{u}_h(\mathbf{y}) = \boldsymbol{\psi}_u(\mathbf{y})\hat{\mathbf{u}}$ be discrete approximations of $\mathbf{u}(\mathbf{y})$. Let the vector $\mathbf{u}$ collect the unknowns $\hat{\mathbf{u}}$. From the stationarity of (5), the linear system

$$\mathbf{M}\mathbf{u} = \mathbf{p} \tag{6}$$

comes out, where

$$\mathbf{M} = \mathscr{A}(\boldsymbol{\psi}_u, \mathscr{M}\boldsymbol{\psi}_u), \quad \mathbf{p} = \mathscr{A}(\boldsymbol{\psi}_u, p).$$

[5]For the hypersingular identity, the boundary limit must be considered at a smooth point $\mathbf{x}^o$ with a well-defined normal vector $\mathbf{n}(\mathbf{x}^o)$ [32].

Please cite this article as: Salvadori A. Infinite boundary elements in 2D elasticity. Eng Anal Bound Elem (2007), doi:10.1016/j.enganabound.2007.06.007

The (symmetric) Galerkin approximation scheme ensures stability and convergence of the numerical solution in suitable functional spaces (for further details see [34]). A major drawback of the method consists in the evaluation of non-integrable kernel $\mathbf{G}_{pp}$, that is, one has to deal with the following form:

$$\int_{\Gamma_p} \psi_k(\mathbf{x}) \int_{\Gamma_p} \mathbf{G}_{pp}(\mathbf{x}-y;\mathbf{n}(\mathbf{x});\mathbf{l}(\mathbf{y}))\psi_h(\mathbf{y})\,\mathrm{d}\Gamma(\mathbf{y})\,\mathrm{d}\Gamma(\mathbf{x}), \tag{7}$$

where $\psi_k(\mathbf{x})$, $\psi_h(\mathbf{y})$ are test and shape functions that model the displacement field on the boundary. The evaluation of (7) is not a trivial task, because of the involved hypersingularities. Several techniques, collectable in three principal groups, have been proposed for their evaluation: (i) regularization techniques, (ii) numerical integrations, (iii) analytical integrations.

2.3. Analytical integrations

Analytical integrations have been basically performed towards three schemes. In the first scheme (see e.g. [35]), the source point is fixed, while the boundary around the source point is temporarily deformed to allow an analytical evaluation of contributions from singular kernels, and then the limit is taken as the deformed boundary shrinks back to the actual boundary. In a second approach, see among others [36], the source point $\mathbf{x}$ is first moved away from the boundary; integrals are evaluated analytically and a limit process is then performed to bring the source point back to the boundary. In all the aforementioned papers, analytical integrations are provided for all singular integrals, while standard quadrature formulae are used for non-singular integrals. In the third scheme, analytical integrations are provided for the complete set of integrals. A complete analytical integration of 2D elastostatic kernels has been provided in [30] for arbitrary degree shape functions on polygonal domains. In the framework of infinite boundary elements, it is necessary to extend analytical integrations in [30] over unbounded domains.

3. Proposal of a polynomial infinite boundary element

Consider a domain T_∞ ($T_\infty \stackrel{def}{=} [x_{10}, \infty[$ in Fig. 1), assumed to be a part of a decomposition Γ_h of a polygonal boundary Γ. A unique polynomial local shape function $\psi_\infty(\mathbf{x})$ of degree n is defined as follows[6]: $\psi_\infty(x_{10}) = 1$; $\psi_\infty(x_1) \in C^{n-1}(T_\infty)$; $supp(\psi_\infty) = [x_{10}, x_\infty]$ where $x_\infty \in R$ is a parameter to be fixed [7] (see Fig. 1).

[6]By definition, $\psi_\infty(x_1)$ has compact support, that does not match with Boussinesque's solution. Shape function $\psi_\infty(x_1)$ may be conceived as a polynomial approximation of Boussinesque's solution on Γ_h.

[7]Parameter x_∞, as shown in the applications that follow, can hardly be identified. Because of such a significant drawback, a polynomial decaying BE seems not to be a suitable choice in spite of its numerical effectiveness.

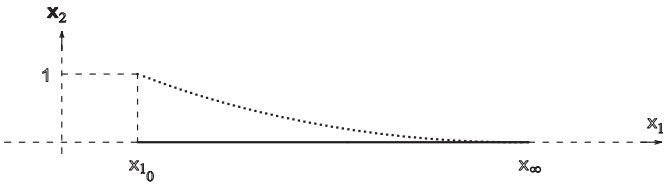

Fig. 1. A polynomial decaying infinite boundary element.

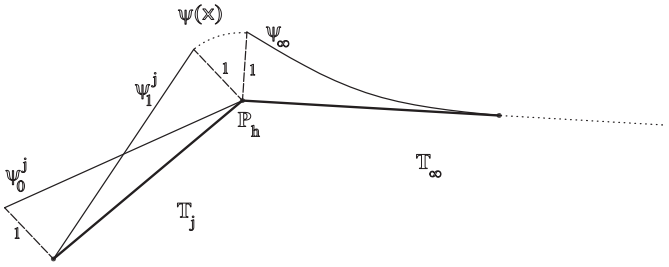

Fig. 2. Local $\psi_\infty(\mathbf{x})$ and global $\psi(\mathbf{x})$ shape functions.

As an example, the quadratic shape function that satisfies all requirements above reads as follows:

$$\psi_\infty(x_1) = 1 - 2\left(\frac{x_1 - x_{10}}{x_\infty - x_{10}}\right) + \left(\frac{x_1 - x_{10}}{x_\infty - x_{10}}\right)^2. \tag{8}$$

Global shape functions ψ_h in Eq. (7) are obtained by collecting in set $\mathscr{T}_h \stackrel{def}{=} \{T_j, T_\infty\}$ the two panels having the common vertex $\mathbf{P}_h$ (see Fig. 2); then ψ_h is defined as

$$\psi_h(\mathbf{y}) \stackrel{def}{=} \begin{cases} \psi_h^j(\mathbf{y}) & \text{if } \mathbf{y} \in T_j, \\ \psi_\infty(\mathbf{y}) & \text{if } \mathbf{y} \in T_\infty, \\ 0 & \text{else,} \end{cases} \tag{9}$$

where ψ_h^j is a usual lagrangian local basis function defined on T_j such that $\psi_h^j(\mathbf{P}_h) = 1$ ($h = 1$ in Fig. 2). By construction, $\psi_h(\mathbf{y})$ is continuous over Γ_h, and its (bounded) support coincides with $\mathscr{T}_h$. In view of the compactness of $\mathscr{T}_h$, making use of analytical integrations [30] that apply to standard polynomial boundary elements is allowable.

4. Proposal of a reciprocal decaying infinite boundary element

4.1. Remarks on the asymptotical behavior of the displacement field

4.1.1. Plane strain finite strip problem

Consider the response of an elastic half-plane made of a homogeneous isotropic material, with Young's modulus E and Poisson's coefficient ν, to the following quasi-static external actions in plane strain hypothesis: a uniformly distributed load p along the boundary for $|x| \leqslant 1$ and a vanishing load elsewhere, as in Fig. 3. By direct integration of the fundamental solution $\mathscr{F}_\sigma(x-\xi, y)$ of Flamant and

Please cite this article as: Salvadori A. Infinite boundary elements in 2D elasticity. Eng Anal Bound Elem (2007), doi:10.1016/j.enganabound.2007.06.007

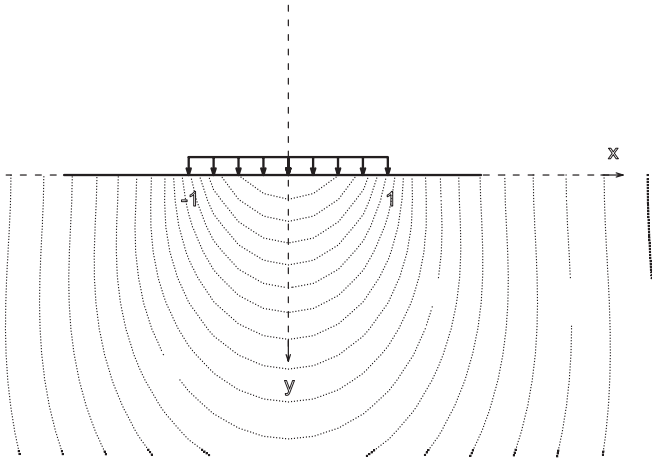

Fig. 3. Boussinesq analysis: problem position and vertical displacement field contour plot.

Boussinesq—see Appendix A

$$\boldsymbol{\sigma}(x,y)=\int_{-1}^{1} p\mathscr{F}_{\sigma}(x-\xi,y)\,\mathrm{d}\xi \tag{10}$$

the analytical solution for the stress tensor $\boldsymbol{\sigma}$ is obtained (see also [23]):

$$\sigma_{xx}=-\frac{p}{\pi}\frac{b(x,y)-a(x,y)}{d^4(x,y)},\quad \sigma_{yy}=-\frac{p}{\pi}\frac{b(x,y)+a(x,y)}{d^4(x,y)}$$
$$\sigma_{xy}=-\frac{p}{\pi}\frac{4xy^2}{d^4(x,y)}, \tag{11}$$

$$\sigma_{zz}=\nu(\sigma_{xx}+\sigma_{yy})$$

having set:

$$d^4(x,y)=((-1+x)^2+y^2)((1+x)^2+y^2),$$

$$a(x,y)=2y(1-x^2+y^2),$$

$$b(x,y)=(x^4+2x^2(-1+y^2)+(1+y^2)^2)\arctan\left(\frac{1-x}{y}\right)+((-1+x^2)^2+2(1+x^2)y^2+y^4)\arctan\left(\frac{1+x}{y}\right).$$

From the expressions above, it can be proved that the stress tensor vanishes at infinity.

In a similar way, by making use of the fundamental solution $\mathscr{F}_u(x-\xi,y)$ of Flamant and Boussinesq [37]—see Appendix A

$$\mathbf{u}(x,y)=\int_{-1}^{1} p\mathscr{F}_u(x-\xi,y)\,\mathrm{d}\xi \tag{12}$$

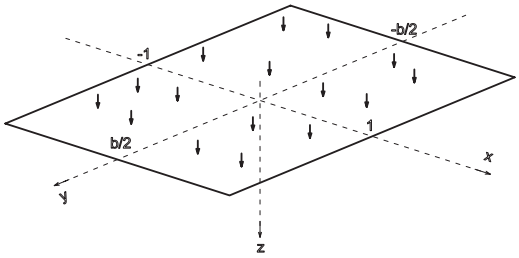

Fig. 4. Rectangular load on an elastic half-space.

the analytical solution for displacements $\mathbf{u}$ comes out:

$$u_x=\kappa\Big\{(2\nu-1)\Big[(-1+x)\arctan\left(\frac{1-x}{y}\right)+(1+x)\arctan\left(\frac{1+x}{y}\right)\Big]+(1-\nu)y\times[\log((1+x)^2+y^2)-\log((-1+x)^2+y^2)]\Big\}, \tag{13a}$$

$$u_y=\kappa\Big\{(2\nu-1)\Big[y\left(\arctan\frac{1-x}{y}+\arctan\frac{1+x}{y}\right)\Big]+(1-\nu)[4+\log(b^4)+(x-1)\log((-1+x)^2+y^2)-(1+x)\log((1+x)^2+y^2)]\Big\} \tag{13b}$$

having set $\kappa=\frac{p}{\pi}\frac{1+\nu}{E}$. In solving a Neumann problem, a rigid body motion remains in the displacement field, which is arbitrary: term $\log(b^2)$ in Eq. (13b) reflects this point. By several authors [3,37,38], b is selected imposing "the distance along the y-axis at which vertical displacement vanishes".[8] Differently from the stress tensor, displacement field $\mathbf{u}$ does not vanish at infinity, giving the paradoxical result that displacements become higher and higher as the distance from the load increases. In spite of Eqs. (13), it is quite common approximating displacement field $\mathbf{u}$ by means of vanishing shape functions, typically of $\frac{1}{r}$ decaying—see [3] for a deep review—but, to the best of our knowledge, no rationale has been proposed to justify this "routine procedure".

In order to further investigate this point, it worths expressing Eqs. (13) on the $y=0$ axis, as follows:

$$u_x=\frac{\pi\kappa}{2}(2\nu-1)[|1+x|-|x-1|], \tag{14a}$$

$$u_y=\kappa(1-\nu)[4+\log(b^4)+(x-1)\log(-1+x)^2-(1+x)\log(1+x)^2]. \tag{14b}$$

4.1.2. Rectangular load on an elastic half-space

Consider the response of an elastic half-space made of a homogeneous isotropic material, with Young's modulus E and Poisson's coefficient ν, to the following quasi-static external actions: a uniformly distributed load p in the

[8] Quite often b is taken as 1, in order to make the expression of $\mathbf{u}(x,y)$ lighter [39].

Please cite this article as: Salvadori A. Infinite boundary elements in 2D elasticity. Eng Anal Bound Elem (2007), doi:10.1016/j.enganabound.2007.06.007

domain $\Omega = \{|\xi| \leqslant 1, |\chi| \leqslant \frac{b}{2}\}$ and a vanishing load elsewhere, as in Fig. 4. The expression of the vertical displacement field along the $y = z = 0$ axis comes out by direct integration of the fundamental solution $\mathscr{B}_{u_z}(x-\xi, y-\chi, z)$ of Boussinesq—see Appendix A

$$u_z(x,y,z;b) = \int_{-b/2}^{b/2}\int_{-1}^{1} p\mathscr{B}_{u_z}(x-\xi, y-\chi, z)\,\mathrm{d}\xi\,\mathrm{d}\chi \tag{15}$$

and it reads as follows:

$$u_z(x, y=0, z=0; b) = \kappa(1-\nu)[l_1(x-1) - l_1(x+1) + l_2(x-1, x+1)] \tag{16}$$

having set:

$$l_1(\alpha) \stackrel{def}{=} \alpha \log \frac{\sqrt{b^2+\alpha^2}-b}{\sqrt{b^2+\alpha^2}+b},$$

$$l_2(\alpha,\beta) \stackrel{def}{=} 2b \log \frac{\sqrt{b^2+\alpha^2}-\alpha}{\sqrt{b^2+\beta^2}-\beta}.$$

It is well known [3] and easily checked from Eq. (16) that, once b is fixed, the displacement field $u_z(x, y=0, z=0; b)$ tends to vanish as $\frac{1}{x}$ when $|x| \to \infty$:

$$u_z(x \to \infty, y=0, z=0; b) = 2\kappa(1-\nu)\frac{b}{x} + O[x^{-2}]. \tag{17}$$

With the aim of a deep understanding of the behavior of the plane strain solution, it is of interest considering the behavior of the vertical displacement field $u_z(x, y=0, z=0; b)$ when b tends to infinity, thus asymptotically reproducing the plain strain conditions. It appears[9] that

$$u_z(x, y=0, z=0; b \to \infty) = \kappa(1-\nu)[4 + \log(b^4) + (x-1)\log(-1+x)^2 - (1+x)\log(1+x)^2]O[b^{-1}] \tag{18}$$

that is, $u_z(x, y=0, z=0; b \to \infty)$ coincides with u_y of Eq. (14b). This conclusion applies also to the more general case of $z \neq 0$, that is $u_z(x, y=0, z; b \to \infty)$ coincides with u_y of Eq. (13b). The extensive expressions of the displacement fields have not been printed here for the sake of brevity.

Eq. (18) gives a deeper insight to the term $\log(b^4)$ in Eqs. (13b)–(14b) due to the meaning of b in the 3D analysis: it plays the role of an unbounded motion that arises in the limit process in Eq. (18) and that applies to all points of the surface $y = 0$, thus making the displacement field unbounded at all points.[10]

It is then possible to build a sequence of functions $u_{z_n} = u_z(x, y=0, z=0; b=n)$ for all $n = 1, 2, \ldots$ and consider if it exists a norm for which u_{z_n} converges[11] to $u_z(x, y=0, z=0; b \to \infty)$. Because $u_z(x, y=0, z=0; b=n)$ vanishes as $|x| \to \infty$ for all n, there is no convergence in the maximum norm.

For the stress field behavior, on the contrary, convergence in the maximum norm holds. Accordingly, it is possible to recover the plain-strain stress field in an elastic half-plane by a limit $b \to \infty$ of stress field $\boldsymbol{\sigma}_b(x,y,z)$ that pertains to the elastic half-space problem depicted in Fig. 4. Such a stress field, parameterized by b, is related to displacement field $u_b(x)$ that vanishes at $|x| \to \infty$ by means of a $\frac{1}{r}$ decaying law.

4.2. Implementation

Consider an unbounded domain T_∞ ($T_\infty \stackrel{def}{=} [x_{10}, \infty[$ in Fig. 1), assumed to be a part of a decomposition Γ_h of a polygonal unbounded boundary Γ. A unique reciprocal decaying local shape function $\psi_\infty(\mathbf{x})$ is defined by

$$\psi_\infty(x_1) = \frac{x_{10}}{x_1}. \tag{19}$$

Global shape functions ψ_h in Eq. (7) are defined again by Eq. (9). By construction, $\psi(\mathbf{x})$ is continuous over Γ_h; its support is unbounded and coincides with $\mathscr{T}_h$.

4.2.1. Lebesgue integrals

In view of the reciprocal decay function (19), analytical integrations performed in [30] do not apply to Eq. (7). The inner "integral" takes the form

$$\int_{\Gamma_p} \mathbf{G}_{pp}(\mathbf{r}; \mathbf{n}(\mathbf{x}); \mathbf{l}(\mathbf{y}))\psi_h(\mathbf{y})\,\mathrm{d}\mathbf{y} = \int_{supp(\psi_h)} \mathbf{G}_{pp}(\mathbf{r}; \mathbf{n}(\mathbf{x}); \mathbf{l}(\mathbf{y}))\psi_h(\mathbf{y})\,\mathrm{d}\mathbf{y} = \mathbf{F}^j_{pp}(\mathbf{x}) + \mathbf{F}^\infty_{pp}(\mathbf{x})$$

having defined $\mathbf{r} = \mathbf{x} - \mathbf{y}$ and

$$\mathbf{F}^k_{pp}(\mathbf{x}) = \int_{T_k} \mathbf{G}_{pp}(\mathbf{r}; \mathbf{n}(\mathbf{x}); \mathbf{l}(\mathbf{y}))\psi_k(\mathbf{y})\,\mathrm{d}\mathbf{y}, \quad k = j, \infty. \tag{20}$$

Integrations performed in [30] apply to integral (20) over T_j. With reference to the remaining integral, analytical integrations will be performed with respect to a bounded domain T^* of length $2l^*$; after having performed the integrations on T^*, integral (20) will be obtained by the limit

$$\mathbf{F}^\infty_{pp}(\mathbf{x}) = \lim_{l^* \to \infty} \int_{T^*} \mathbf{G}_{pp}(\mathbf{r}; \mathbf{n}(\mathbf{x}); \mathbf{l}(\mathbf{y}))\psi_\infty(\mathbf{y})\,\mathrm{d}\mathbf{y}. \tag{21}$$

To this aim, let $\mathscr{L} \equiv \{y_1, y_2\}$ define a local c.s. with origin in the midpoint of T^*, oriented as in Fig. 5. If $\mathbf{y} \in T^*$ then $\mathbf{l}(\mathbf{y}) = (0,1)$, $y_2 = 0$, $-l^* \leqslant y_1 \leqslant l^*$ and $\psi_\infty(\mathbf{y}) = \frac{y_{10}}{y_{10}+y_1+l^*}$.

[9] All mathematical steps have been conducted via Mathematica. The corresponding subroutines are presented in Appendix B.

[10] This observation is in agreement with the remark by [40]: "unbounded plane stress and plane strain domains subjected to static loading undergo infinite displacements, even when the zero displacement boundary condition at infinity is enforced." and with the examples described therein (axial rod with varying sections). While the displacement field is unbounded in all the domain, and zero at infinity, relative displacements, stress and strain fields are well behaved.

[11] This path of reasoning gives a rationale to the use of vanishing displacement fields in approximating the stress distribution in plane strain unbounded domain problems, which is a rather "standard procedure" in finite as well as in boundary element simulations.

Please cite this article as: Salvadori A. Infinite boundary elements in 2D elasticity. Eng Anal Bound Elem (2007), doi:10.1016/j.enganabound.2007.06.007

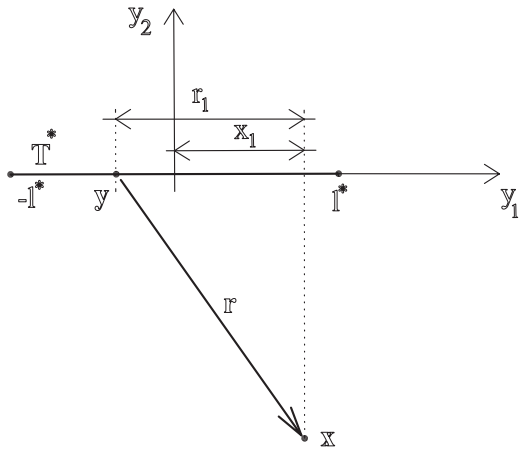

Fig. 5. Local coordinate system $\mathscr{L}$.

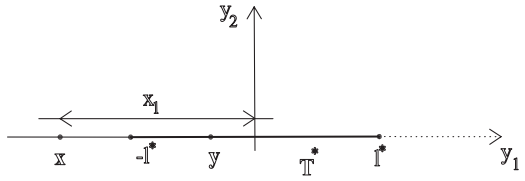

Fig. 6. $\mathbf{x} \notin T_i$, but $x_2 = 0$.

By the change of variable $y_1 = x_1 - r_1$, Eq. (20) becomes

$$\mathbf{F}^*_{pp}(\mathbf{x}) = \int_{x_1-l^*}^{x_1+l^*} \mathbf{G}_{pp}(\mathbf{r}) \frac{y_{10}}{z_1 - r_1} \, \mathrm{d}r_1 \Big|_{r_2=x_2} \tag{22}$$

having set $z_1 \overset{def}{=} y_{10} + x_1 + l^*$. Integral (22) depends on the position of the point $\mathbf{x}$ with respect to T^*. Kernel $\mathbf{G}_{pp}(\mathbf{x}-\mathbf{y}, \mathbf{n}(\mathbf{x}), \mathbf{l}(\mathbf{y}))$ is *singular with respect to* $\mathbf{y}$ depending on the position of $\mathbf{x}$ with respect to T^*. The two items $\mathbf{x} \notin T^*$ and $\mathbf{x} \in T^*$ must be accordingly separately discussed.

Easy algebraic manipulations lead from integral (22) to the following basic integrals:

$$\int_{x_1-l^*}^{x_1+l^*} \frac{1}{r^2} \frac{1}{z_1 - r_1} \, \mathrm{d}r_1,$$
$$\int_{x_1-l^*}^{x_1+l^*} \frac{1}{r^4} \frac{r_1^k}{z_1 - r_1} \, \mathrm{d}r_1, \quad k = 0, 1, 2,$$
$$\int_{x_1-l^*}^{x_1+l^*} \frac{1}{r^6} \frac{r_1^k}{z_1 - r_1} \, \mathrm{d}r_1, \quad k = 0, 1, 2, 3,$$

where $r^2 = r_1^2 + r_2^2$. They have been analytically solved when $\mathbf{x} \notin T^*$ (results in Appendix D). Collecting all common terms, integral (22) reads as follows:

$$\mathbf{F}^*_{pp}(\mathbf{x}) = y_{10} \left[\mathbf{L}_{pp} \log \frac{r^2}{(z_1 - r_1)^2} + \mathbf{A}_{pp} \arctan \frac{r_1}{x_2} + \frac{1}{r^2} \mathbf{S}_{pp} + \frac{1}{r^4} \mathbf{H}_{pp} \right]_{r_1=x_1-l^*}^{r_1=x_1+l^*}, \tag{23}$$

where $\mathbf{L}_{pp}$, $\mathbf{A}_{pp}$, $\mathbf{S}_{pp}$, and $\mathbf{H}_{pp}$, are suitable matrices[12] collected in Appendix E

As a particular instance of $\mathbf{x} \notin T_i$, consider $x_2 = 0$ (see Fig. 6). The expression of hypersingular kernel $\mathbf{G}_{pp}$ simplifies being $x_2 = 0$ and $\mathbf{r} \cdot \mathbf{l} = 0$.

$$\mathbf{G}_{pp}(\mathbf{x}-\mathbf{y}, \mathbf{n}(\mathbf{x}), \mathbf{l}(\mathbf{y})) = \frac{G}{2\pi} \frac{1}{1-\nu} \begin{pmatrix} n_2 & n_1 \\ n_1 & n_2 \end{pmatrix} \frac{1}{r_1^2}. \tag{24}$$

Eq. (23) specifies as

$$\mathbf{F}^*_{pp}(\mathbf{x}) = y_{10} \frac{G}{2\pi} \frac{1}{1-\nu} \begin{pmatrix} n_2 & n_1 \\ n_1 & n_2 \end{pmatrix} \times \left[\frac{1}{z_1^2} \log \frac{r_1}{r_1 - z_1} - \frac{1}{r_1 z_1} \right]_{r_1=x_1-l^*}^{r_1=x_1+l^*}. \tag{25}$$

4.2.2. Hadamard's finite part

Consider

$$\begin{aligned} I(\varepsilon) &= \int_{x_1-l^*}^{-\varepsilon} \frac{1}{r_1^2} \frac{1}{z_1 - r_1} \, \mathrm{d}r_1 + \int_{\varepsilon}^{x_1+l^*} \frac{1}{r_1^2} \frac{1}{z_1 - r_1} \, \mathrm{d}r_1 \\ &= \left[\frac{1}{z_1^2} \log \frac{r_1}{r_1 - z_1} - \frac{1}{r_1 z_1} \right]_{r_1=x_1-l^*}^{r_1=-\varepsilon} \\ &\quad + \left[\frac{1}{z_1^2} \log \frac{r_1}{r_1 - z_1} - \frac{1}{r_1 z_1} \right]_{r_1=\varepsilon}^{r_1=x_1+l^*} \\ &= \left[\frac{1}{z_1^2} \log \frac{r_1}{r_1 - z_1} - \frac{1}{r_1 z_1} \right]_{r_1=x_1-l^*}^{r_1=x_1+l^*} \\ &\quad + \frac{2}{\varepsilon z_1} + \frac{1}{2z_1^2} \log \frac{(\varepsilon - z_1)^2}{(\varepsilon + z_1)^2}. \end{aligned}$$

By taking the limit $\varepsilon \to 0^+$ integral $I(\varepsilon)$ becomes

$$\lim_{\varepsilon \to 0^+} I(\varepsilon) = \left[\frac{1}{z_1^2} \log \frac{r_1}{r_1 - z_1} - \frac{1}{r_1 z_1} \right]_{r_1=x_1-l^*}^{r_1=x_1+l^*} + \lim_{\varepsilon \to 0^+} \frac{2}{\varepsilon z_1}.$$

By definition of finite part of Hadamard of divergent integral $I(\varepsilon)$ (see [41, p. 16]), it turns out:

$$\oint_{x_1-l^*}^{x_1+l^*} \frac{1}{r_1^2} \frac{1}{z_1 - r_1} \, \mathrm{d}r_1 = \left[\frac{1}{z_1^2} \log \frac{r_1}{r_1 - z_1} - \frac{1}{r_1 z_1} \right]_{r_1=x_1-l^*}^{r_1=x_1+l^*}. \tag{26}$$

In view of (26), it is then proved that the finite part of Hadamard of integral (22) when $\mathbf{x} \in T_\infty$ coincides with expression (25).

Considering a different approach to boundary integral equations, the so-called "limit to the boundary" technique [36], the limit to the boundary process $\mathbf{F}^*_{pp}(\mathbf{z})$ s.t. $T_\infty \ni \mathbf{z} \to \mathbf{x} \in T_\infty$ can be performed. By taking $x_2 \to 0^-$ and

[12] Their expressions have been evaluated by means of the commercial code MATHEMATICA 4.0.

Please cite this article as: Salvadori A. Infinite boundary elements in 2D elasticity. Eng Anal Bound Elem (2007), doi:10.1016/j.enganabound.2007.06.007

setting[13] $\mathbf{n}(\mathbf{x}) = (0,1)$, it holds:

$$\lim_{x_2\to 0^-} \mathbf{L}_{pp} = \frac{G}{4\pi(1-\nu)}\frac{1}{z_1^2}\begin{pmatrix}1 & 0\\ 0 & 1\end{pmatrix},$$

$$\lim_{x_2\to 0^-} \mathbf{A}_{pp} = \mathbf{0},$$

$$\lim_{x_2\to 0^-} \mathbf{S}_{pp} = -\frac{G}{2\pi(1-\nu)}\frac{1}{r_1 z_1}\begin{pmatrix}1 & 0\\ 0 & 1\end{pmatrix},$$

$$\lim_{x_2\to 0^-} \mathbf{H}_{pp} = \mathbf{0}.$$

Eq. (25) is obtained immediately from (23).

One concludes therefore that when $\mathbf{x}\notin \bar{T}_j$, the hypersingularities in integral (22) are not triggered off and $\mathbf{F}^*_{pp}(\mathbf{x})$ is a classical Lebesgue integral. On the contrary, as $\mathbf{x}\in T_j$ "integral" (22) does not exist in a Lebesgue sense but it assumes the distributional nature of finite part of Hadamard. In a different approach, the same result is obtained by limit to the boundary process.

4.2.3. Unbounded domain

Consider limit (21), that is

$$\mathbf{F}^{\infty}_{pp}(\mathbf{x}) = \lim_{l^*\to\infty} \mathbf{F}^*_{pp}(\mathbf{x}).$$

From the definition of local coordinate system $\mathscr{L}$, $l^*\to\infty$ implies $x_1 - l^*\to\infty$, whereas $x_1 + l^*$ as well as z_1 are constants that do not depend on l^*. Matrices $\mathbf{S}_{pp}$ and $\mathbf{H}_{pp}$ (see Appendix E) permit to prove that

$$\lim_{l^*\to\infty}\left[\frac{1}{r^2}\mathbf{S}_{pp} + \frac{1}{r^4}\mathbf{H}_{pp}\right]_{r_1=x_1-l^*} = \mathbf{0}.$$

Moreover, since matrices $\mathbf{L}_{pp}$, $\mathbf{A}_{pp}$ do not depend on r_1, it is straightforward to show that

$$\lim_{l^*\to\infty}\left[\mathbf{L}_{pp}\log\frac{r^2}{(z_1-r_1)^2}\right]_{r_1=x_1-l^*} = \mathbf{0}$$

and that, being $x_2\leqslant 0$ in $\mathscr{L}$,

$$\lim_{l^*\to\infty}\left[\mathbf{A}_{pp}\arctan\frac{r_1}{x_2}\right]_{r_1=x_1-l^*} = -\frac{\pi}{2}\mathbf{A}_{pp}.$$

One concludes therefore that

$$\mathbf{F}^{\infty}_{pp}(\mathbf{x}) = y_{10}\left\{\left[\mathbf{L}_{pp}\log\frac{r^2}{(z_1-r_1)^2} + \mathbf{A}_{pp}\arctan\frac{r_1}{x_2} + \frac{1}{r^2}\mathbf{S}_{pp} + \frac{1}{r^4}\mathbf{H}_{pp}\right]^{r_1=x_1+l^*} - \frac{\pi}{2}\mathbf{A}_{pp}\right\}. \tag{27}$$

5. Proposal of a constant-logarithmic infinite boundary element: hypersingular collocation approach

Consider an unbounded domain T_∞ ($T_\infty \overset{def}{=} [y_{10},\infty[$ in Fig. 1), assumed to be a part of a decomposition Γ_h of a polygonal unbounded boundary Γ. In order to approximate problem (1) via the hypersingular collocation approach, consider a matrix of shape functions $\boldsymbol{\psi}^{\infty}_h(\mathbf{y})$ defined over T_∞ as

$$\boldsymbol{\psi}^{\infty}_h(\mathbf{y}) \overset{def}{=} \begin{pmatrix}\psi_1(\mathbf{y}) & 0\\ 0 & \psi_2(\mathbf{y})\end{pmatrix} \tag{28}$$

thus allowing shape function $\psi_1(\mathbf{y})$ in direction y_1 to be different from $\psi_2(\mathbf{y})$ in direction y_2. Let $\psi_1(\mathbf{y})$ reproduce the constant asymptotical behavior of Eq. (14a) and $\psi_2(\mathbf{y})$ reproduce the asymptotical logarithmic behavior of Eq. (14b), that is assume in a global coordinate system:

$$\psi_1(y) = 1, \quad \psi_2(y) = \log\left(e\,\frac{y}{y_{10}}\right), \tag{29}$$

where e stands for Nepero's number. Global shape functions $\boldsymbol{\psi}_h$ in Eq. (7) are defined again as in Eq. (9). By construction, $\boldsymbol{\psi}_h(\mathbf{y})$ are continuous over Γ_h; their support is unbounded and coincides with $\mathscr{T}_h$.

5.1. Constant shape function

Analytical integrations for constant shape functions on bounded domains have been performed in [30]. By assuming for the unbounded domain the path of reasoning and notation of Section 4.2.3, it is straightforward to get

$$\int_{T_\infty}\mathbf{G}_{pp}(\mathbf{r};\mathbf{n}(\mathbf{x});\mathbf{l}(\mathbf{y}))\psi_1(\mathbf{y})\,\mathrm{d}\mathbf{y} = \frac{G}{4\pi}\frac{1}{1-\nu}\left[\frac{1}{r^2}\mathbf{S}_{pp} + \frac{1}{r^4}\mathbf{H}_{pp}\right]^{r_1=x_1+l^*} \tag{30}$$

with $r_2 = x_2$ and

$$\mathbf{S}_{pp} = -2\begin{pmatrix}n_2r_1 - 3n_1r_2 & \mathbf{r}\cdot\mathbf{n},\\ \mathbf{r}\cdot\mathbf{n} & n_2r_1 + n_1r_2\end{pmatrix}^{r_1=x_1+l^*},$$

$$\mathbf{H}_{pp} = 4r_2^2\begin{pmatrix}n_2r_1 - n_1r_2 & \mathbf{r}\cdot\mathbf{n}\\ \mathbf{r}\cdot\mathbf{n} & -n_2r_1 + n_1r_2\end{pmatrix}^{r_1=x_1+l^*}.$$

5.2. Logarithmic shape function

5.2.1. Hadamard's finite part

Assume for the unbounded domain the path of reasoning and notation of Section 4.2.3. Furthermore, as a particular instance of $\mathbf{x}\notin T_\infty$, consider $x_2 = 0$ (see Fig. 6). The expression of hypersingular kernel $\mathbf{G}_{pp}$ simplifies as in Eq. (24) and analytical integration can be performed by splitting in the local reference $\mathscr{L}$

$$\psi_2(y) = \log\left(\frac{e}{y_{10}}\right) + \log(z_1 - r_1)$$

[13] A free term comes into play in the limit process if $n_1\neq 0$: for details onto this point see [42].

with $z_1 = x_1 + y_{10} + l^*$. Integrating the constant factor as in Eq. (30), straightforwardly one gets

$$\int_{T_\infty} \mathbf{G}_{pp}(\mathbf{r};\mathbf{n}(\mathbf{x});\mathbf{l}(\mathbf{y}))\log(z_1 - r_1)\,\mathrm{d}\mathbf{y} =$$
$$z_1 \neq 0 \rightarrow -\frac{G}{4\pi}\frac{1}{1-\nu}\begin{pmatrix} n_2 & n_1 \\ n_1 & n_2 \end{pmatrix} \left[\frac{r_1\log(r_1^2) + y_{10}\log(y_{10}^2)}{r_1(r_1+y_{10})}\right]^{r_1=x_1+l^*}$$
$$z_1 = 0 \rightarrow -\frac{G}{4\pi}\frac{1}{1-\nu}\begin{pmatrix} n_2 & n_1 \\ n_1 & n_2 \end{pmatrix} \times \left[\frac{2+\log(r_1^2)}{r_1}\right]^{r_1=x_1+l^*}. \tag{31}$$

By the same path of reasoning of Section 4.2.2, it can be proved that the finite part of Hadamard of integral reads as follows:

$$\oint\!\!\!\!\!\!= \int_{T_\infty} \mathbf{G}_{pp}(\mathbf{r};\mathbf{n}(\mathbf{x});\mathbf{l}(\mathbf{y}))\psi_2(\mathbf{y})\,\mathrm{d}\mathbf{y}$$
$$= -\frac{G}{4\pi}\frac{1}{1-\nu}\begin{pmatrix} n_2 & n_1 \\ n_1 & n_2 \end{pmatrix} \times \left[\frac{2\log\left(\frac{e}{y_{10}}\right)}{r_1} + \frac{r_1\log(r_1^2) + y_{10}\log(y_{10}^2)}{r_1(r_1+y_{10})}\right]^{r_1=x_1+l^*}.$$

5.2.2. Lebesgue integrals approximation

It has not been possible to find out a closed form of integral (7) for logarithmic shape function $\psi_2(\mathbf{y})$ when $x_2 \neq 0$ in local reference $\mathscr{L}$ defined in Section 4. Accordingly, integral (7) has been approximated as follows. By the change of variable $y_1 = x_1 - r_1$ it comes out:

$$\int_{T_\infty} \mathbf{G}_{pp}(\mathbf{r};\mathbf{n}(\mathbf{x});\mathbf{l}(\mathbf{y}))\psi_2(\mathbf{y})\,\mathrm{d}\mathbf{y} = \int_{-\infty}^{x_1-y_{10}} \mathbf{G}_{pp}(\mathbf{r};\mathbf{n}(\mathbf{x});\mathbf{l}(\mathbf{y}))\log\left(e\,\frac{x_1-r_1}{y_{10}}\right)\mathrm{d}r_1.$$

If $x_1 - y_{10} > 0$, the last integral can be split into two parts:

$$\int_{-\infty}^{0} \mathbf{G}_{pp}(\mathbf{r};\mathbf{n}(\mathbf{x});\mathbf{l}(\mathbf{y}))\log\left(e\,\frac{x_1-r_1}{y_{10}}\right)\mathrm{d}r_1 + \int_{0}^{x_1-y_{10}} \mathbf{G}_{pp}(\mathbf{r};\mathbf{n}(\mathbf{x});\mathbf{l}(\mathbf{y}))\log\left(e\,\frac{x_1-r_1}{y_{10}}\right)\mathrm{d}r_1$$

and by the variable change

$$r_1 = -\sqrt{r_2^2\left(\frac{1}{\eta^2}-1\right)}$$

they become

$$\int_0^1 \hat{\mathbf{G}}_{pp}(\mathbf{r}(\eta);\mathbf{n}(\mathbf{x});\mathbf{l}(\mathbf{y}))\log\left[\left(x_1 + \sqrt{r_2^2\left(\frac{1}{\eta^2}-1\right)}\right)\frac{e}{y_{10}}\right] \times \frac{1}{|r_2|}\frac{1}{\sqrt{1-\eta^2}}\,\mathrm{d}\eta + \int_0^{x_1-y_{10}} \mathbf{G}_{pp}(\mathbf{r};\mathbf{n}(\mathbf{x});\mathbf{l}(\mathbf{y}))\log\left(e\,\frac{x_1-r_1}{y_{10}}\right)\mathrm{d}r_1 \tag{32}$$

having defined by $\hat{\mathbf{G}}_{pp}$ the smooth function:

$$\hat{\mathbf{G}}_{pp}(\mathbf{r}(\eta);\mathbf{n}(\mathbf{x});\mathbf{l}(\mathbf{y})) = (\mathbf{r}\cdot\mathbf{r})\;\mathbf{G}_{pp}(\mathbf{r}(\eta);\mathbf{n}(\mathbf{x});\mathbf{l}(\mathbf{y})).$$

The latter factor in Eq. (32) shows no singularity and can be approximated by a usual Gauss quadrature rule. The former integral shows two weak boundary singularities, with different nature: at $\eta = 0$ the argument of the logarithm becomes undefined, whereas at $\eta = 1$ the argument of the square root at the denominator vanishes. Both singularities can be efficiently approximated by means of smoothing transformations, as proposed in [31].

6. A benchmark: plane strain finite strip problem

Consider the problem described in Section 4.1, with a uniformly distributed load of $p = 1\,\mathrm{daN/m}$ over a finite strip of 2 m. The assumed material parameters are as follows: $E = 540\,\mathrm{MPa}$, $\nu = 0.35$. Finite element analysis (via the commercial code Abaqus [6]) as well as hypersingular collocation boundary element analysis (via a self-implemented computer code) have been considered; comparisons have been made in terms of the stress components at point $P = (0,1)$ (coordinates in meters). The relative error in evaluating the components σ_{xx} and σ_{yy} is plotted with reference to a square region, in order to show the overall precision of the two techniques.

6.1. Boundary elements analyses

BE analyses have been carried out in three steps. First, a mesh calibration has been performed within the load-strip, in the so-called core region [22], making use of no elements outside it, neither finite nor infinite.

Table 1
Numerical approximation of stresses at points $A(0,1)$, $B(1,1)$, and $C(1,10)$ via collocation BEM

	Point $A(0,1)$			Point $B(1,1)$			Point $C(1,10)$		
	σ_{xx}	σ_{xy}	σ_{yy}	σ_{xx}	σ_{xy}	σ_{yy}	σ_{xx}	σ_{xy}	σ_{yy}
An.	−0.182	0	−0.818	−0.225	0.255	−0.480	−0.00162	0.01224	−0.1240
1	−0.014	–	−0.722	−0.091	0.318	−0.311	0.00960	0.00732	−0.0644
2	0.014	–	−0.748	−0.103	0.302	−0.269	0.00931	0.00713	−0.0634
4	0.016	–	−0.733	−0.104	0.293	−0.256	0.00912	0.00702	−0.0628
8	0.016	–	−0.721	−0.103	0.287	−0.252	0.00901	0.00695	−0.0625
16	0.017	–	−0.714	−0.103	0.283	−0.250	0.00895	0.00691	−0.0623
32	0.017	–	−0.710	−0.102	0.281	−0.248	0.00891	0.00688	−0.0622
64	0.017	–	−0.709	−0.102	0.280	−0.247	0.00890	0.00687	−0.0621

Please cite this article as: Salvadori A. Infinite boundary elements in 2D elasticity. Eng Anal Bound Elem (2007), doi:10.1016/j.enganabound.2007.06.007

Table 2
Numerical approximation at points $A(0,1)$, $B(1,1)$, and $C(1,10)$ via collocation BEM

Γ	#BE	Point $A(0,1)$			Point $B(1,1)$			Point $C(1,10)$		
		σ_{xx}	σ_{xy}	σ_{yy}	σ_{xx}	σ_{xy}	σ_{yy}	σ_{xx}	σ_{xy}	σ_{yy}
$[-1,1]$	16	0.017		−0.714	−0.103	0.283	−0.250	8.95E − 03	6.91E − 03	−6.23E − 02
$[-3,3]$	48	−0.115		−0.825	−0.146	0.269	−0.493	1.48E − 02	1.07E − 02	−8.43E − 02
$[-5,5]$	80	−0.150		−0.829	−0.185	0.259	−0.500	1.79E − 02	1.27E − 02	−9.85E − 02
$[-10,10]$	160	−0.173		−0.830	−0.210	0.257	−0.501	1.78E − 02	1.37E − 02	−1.18E − 01
$[-20,20]$	320	−0.183		−0.830	−0.220	0.257	−0.501	1.03E − 02	1.30E − 02	−1.26E − 01
	An.	−0.182		−0.818	−0.225	0.255	−0.480	−1.62E − 03	1.22E − 02	−1.24E − 01

Table 3
Numerical approximation of stresses at points $A(0,1)$, $B(1,1)$, and $C(1,10)$ via collocation BEM

Γ	#BE	Point $A(0,1)$			Point $B(1,1)$			Point $C(1,10)$		
		σ_{xx}	σ_{xy}	σ_{yy}	σ_{xx}	σ_{xy}	σ_{yy}	σ_{xx}	σ_{xy}	σ_{yy}
$[-1,1]$	32	0.017		−0.710	−0.102	0.281	−0.248	0.009	0.007	−0.062
$[-5,5]$	96	−0.151		−0.829	−0.185	0.259	−0.503	0.018	0.013	−0.099
$[-13,13]$	160	−0.179		−0.830	−0.215	0.256	−0.504	0.015	0.013	−0.123
$[-29,29]$	224	−0.187		−0.830	−0.223	0.256	−0.504	0.006	0.013	−0.128
$[-61,61]$	288	−0.190		−0.830	−0.226	0.256	−0.504	0.002	0.013	-0.128
	An.	−0.182		−0.818	−0.225	0.255	−0.480	−1.62E − 03	1.22E − 02	−1.24E − 01

Table 4
Fine mesh

Intervals	$[-61,-29]$	$[-29,-13]$	$[-13,-5]$	$[-5,-2]$	$[-2,-1]$	$[-1,1]$	$[1,2]$	$[2,5]$	$[5,13]$	$[13,29]$	$[29,61]$
BEM	32	32	32	24	16	64	16	24	32	32	32
Length	1	1/2	1/4	1/8	1/16	1/32	1/16	1/8	1/4	1/2	1
#1					336 BE						
#2					272 BE						
#3					208 BE						
#4					144 BE						
#5					168 BE						

Table 5
Numerical approximation of stresses at points $A(0,1)$, $B(1,1)$, and $C(1,10)$ via collocation BEM

Mesh	Point $A(0,1)$			Point $B(1,1)$			Point $C(1,10)$		
	σ_{xx}	σ_{xy}	σ_{yy}	σ_{xx}	σ_{xy}	σ_{yy}	σ_{xx}	σ_{xy}	σ_{yy}
#4	−0.146		−0.824	−0.184	0.258	−0.491	0.01774	0.01257	−0.097
#3	−0.174		−0.824	−0.213	0.256	−0.492	0.01523	0.01326	−0.121
#2	−0.182		−0.824	−0.221	0.256	−0.492	0.00623	0.01257	−0.126
#1	−0.185		−0.824	−0.224	0.256	−0.492	0.002	0.012	−0.126
An.	−0.182		−0.818	−0.225	0.255	−0.480	−1.62E − 03	1.22E − 02	−1.24E − 01
% err	1.66		0.75	0.36	0.46	2.48	–	1.69	1.43

Table 1 compares the analytical solution (Eq. (11)) and the numerical approximation via the standard collocation BEM on a uniform discretization of the core region made of 2^n linear boundary elements, $n = 0, 1, \ldots, 6$. It shows that the unbounded boundary outside of the core region plays a major role in the stress analysis under the load strip, measured at points $A(0,1)$, $B(1,1)$, and $C(1,10)$. In Table 2 the uniformly discretized domain consists of elements of $\frac{1}{8}$

Please cite this article as: Salvadori A. Infinite boundary elements in 2D elasticity. Eng Anal Bound Elem (2007), doi:10.1016/j.enganabound.2007.06.007

Table 6
Benchmark on the characteristic length x_∞

		Point $A(0,1)$			Point $B(1,1)$			Point $C(1,10)$		
		σ_{xx}	σ_{xy}	σ_{yy}	σ_{xx}	σ_{xy}	σ_{yy}	σ_{xx}	σ_{xy}	σ_{yy}
Mesh #4		−0.146		−0.824	−0.184	0.258	−0.491	0.01774	0.01257	−0.097
x_∞	13	−0.165		−0.824	−0.205	0.256	−0.491	0.01781	0.01344	−0.113
	29	−0.177		−0.824	−0.216	0.256	−0.492	0.01082	0.01284	−0.125
	61	−0.184		−0.824	−0.223	0.256	−0.492	0.00036	0.01213	−0.131
	100	−0.187		−0.825	−0.227	0.256	−0.492	−0.0066	0.01179	−0.134
	1000	−0.194		−0.825	−0.234	0.256	−0.492	−0.0281	0.01102	−0.140

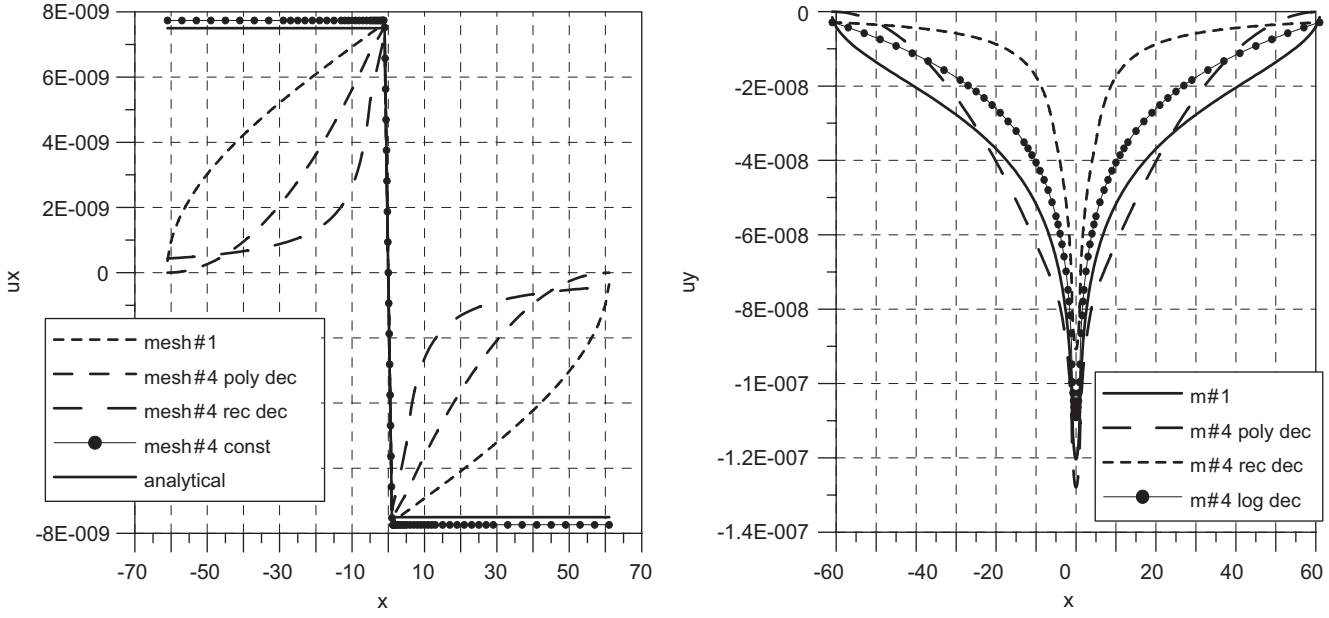

Fig. 7. Displacement field along the boundary.

length. The first row coincides with sixth row in Table 1, that is merely the core region has been discretized; the second row refers to a discretization of 48 boundary elements, that is the interval $[-3,3]$ along the x-axis has been discretized, and so on. Table 2 shows, as expected, that uniform meshes are not the best choice for this class of problems. In order to obtain good approximations in the vicinity of the load strip, fine meshes are required in the core region. On the other hand, in the far field, coarse meshes permit to enlarge the discretized domain without loss of accuracy in the region where stresses are higher. This is clearly stated in Table 3 in which 32 boundary elements of different lengths are considered in intervals $[-61,-29]$, $[-29,-13]$, $[-13,-5]$, $[-5,-1]$, $[-1,1]$ and their positive counterparts. More accurate results have been obtained from the last analysis ($\Gamma=[-61,61]$) by refining the mesh around and inside the core region. Five meshes are described in Table 4: meshes #1 to #4 have the same discretization in the overlapping region and differ as to the extension of the modeled surface. Mesh #5 differs from mesh #4 by a finer discretization around the two nodes where a jump in the distributed load comes into play. Results obtained with meshes #1 to #4 are collected in Table 5: relative error pertains to mesh #1.

As a second step in boundary elements numerical analysis, infinite polynomial BE have been used in mesh #4, that, as seen in Table 4, is defined on interval $[-5,5]$ by 144 boundary elements. Polynomial decaying infinite elements are characterized by the unknown length x_∞, which optimal value might be identified by the obtained accuracy: this is the goal of Table 6. It is remarkable that at $x_\infty=61$ results show a comparable accuracy with results obtained with mesh #1. Accordingly, the polynomial decaying element reveals effective since it is "accuracy equivalent" to 96 boundary elements. Notwithstanding, the accuracy decreases as expected when x_∞ becomes too high, since the shape function (8) fails to simulate the right solution behavior. As a consequence, an optimal length for

Please cite this article as: Salvadori A. Infinite boundary elements in 2D elasticity. Eng Anal Bound Elem (2007), doi:10.1016/j.enganabound.2007.06.007

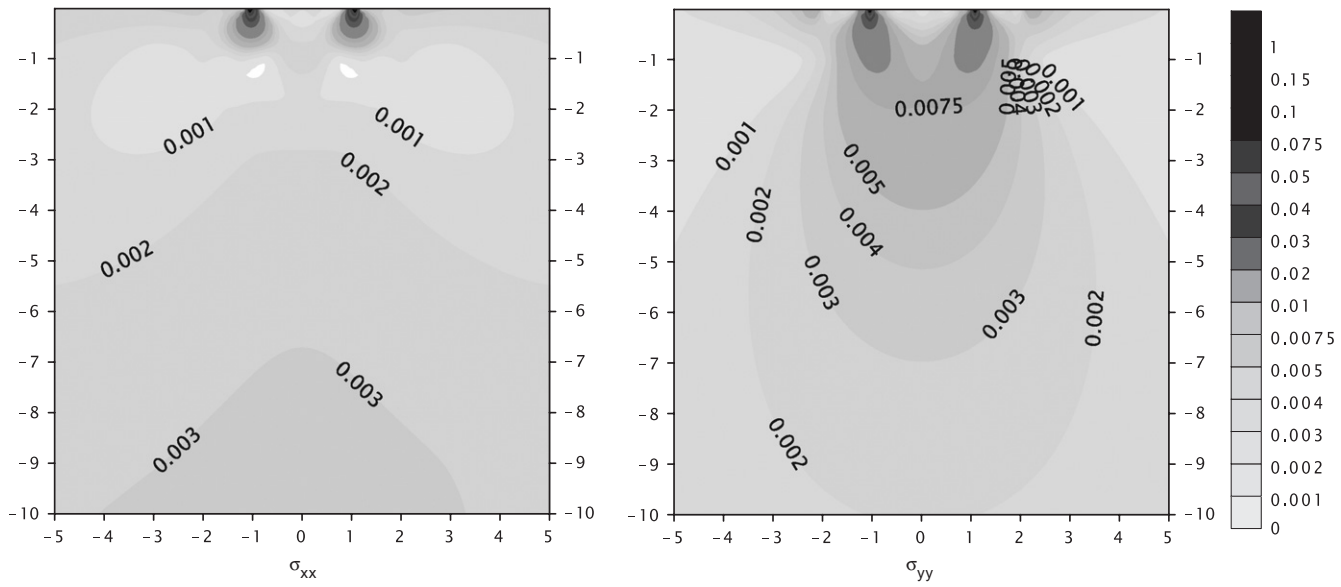

Fig. 8. Absolute error on the stress field in the core region by using the polynomial infinite boundary element on mesh #4.

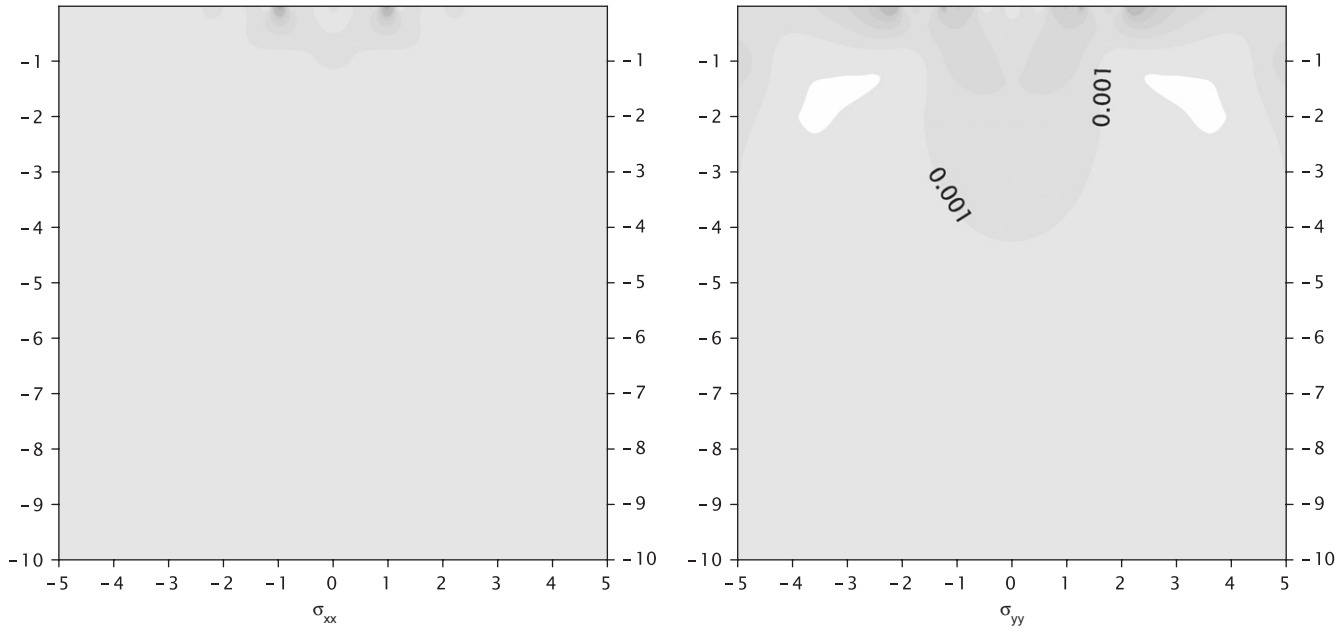

Fig. 9. Absolute error on the stress field in the core region by using the const log infinite boundary element on mesh #5 (color levels as in Fig. 8).

x_∞ must be selected, which depends on the problem. Such a parameter seems to be hardly identifiable for any problem: polynomial decaying boundary elements seems therefore to be unsuitable.

Further numerical analyses have been performed with reciprocal decaying as well as with const/log infinite boundary elements. A comparison in terms of the displacement field on the boundary for meshes #1 and #4 by making use of all proposed infinite elements [14] is plotted in Fig. 7: only the const–log element captures well the exact behavior of horizontal displacements, which is not vanishing at infinity. On the contrary, all elements reproduce quite similarly the vertical displacement field along the boundary of the core region.

Fig. 8 shows the absolute error in stress within the core region due to mesh #4 with polynomial decaying infinite elements when $x_\infty = 61$. The absolute error manifests a peak around the discontinuity of the external load: this evidence lead to refine the discretization around these points (mesh #5), in order to decrease the error peak.

[14] $x_\infty = 61$ for polynomial infinite elements.

Please cite this article as: Salvadori A. Infinite boundary elements in 2D elasticity. Eng Anal Bound Elem (2007), doi:10.1016/j.enganabound.2007.06.007

Table 7
Numerical approximation via collocation BEM

Mesh	∞ element	$A(0,1)$			$B(1,1)$		
		σ_{xx}	σ_{xy}	σ_{yy}	σ_{xx}	σ_{xy}	σ_{yy}
#5	None	−0.142		−0.819	−0.183	0.256	−0.481
#5	Reciprocal	−0.165		−0.819	−0.208	0.256	−0.482
#5	Const/log	−0.182		−0.820	−0.225	0.256	−0.482
An.		−0.182		−0.818	−0.225	0.255	−0.480
		$C(1,10)$			$D(10,1)$		
Mesh	∞ element	σ_{xx}	σ_{xy}	σ_{yy}	σ_{xx}	σ_{xy}	σ_{yy}
#5	None	0.017	0.01213	−0.095	0.0130	0.00481	0.0180
#5	Reciprocal	0.0135	0.0131	−0.114	0.0127	0.00408	0.0207
#5	Const/log	−0.0017	0.0124	−0.124	−0.127	0.00129	−0.000273
An.		−0.00162	0.0122	−0.124	−0.126	0.00127	−0.000129

Table 8
Comparison in terms of accuracy at $P = (0,1)$

Analysis	σ_{xx} (daN/m^2)	% error	σ_{yy} (daN/m^2)	% error
Analytical	−0.18169	–	−0.81831	–
FEM				
#1	−0.0691 −0.095 −0.095 −0.0691	55	−0.8050 −0.8406 −0.8406 −0.8050	0.55
#2	−0.1181 −0.1424 −0.1424 −0.1181	28	−0.8013 −0.8366 −0.8366 −0.8013	0.08
#3	−0.1417 −0.1150 −0.1150 −0.1417	29	−0.8374 −0.8010 −0.8010 −0.8374	0.11
#4	−0.1584 −0.1321 −0.1321 −0.1584	20	−0.8368 −0.8005 −0.8005 −0.8368	0.04
#5	−0.1632 −0.1905 −0.1905 −0.1632	3	−0.7998 −0.8366 −0.8366 −0.7998	0.01

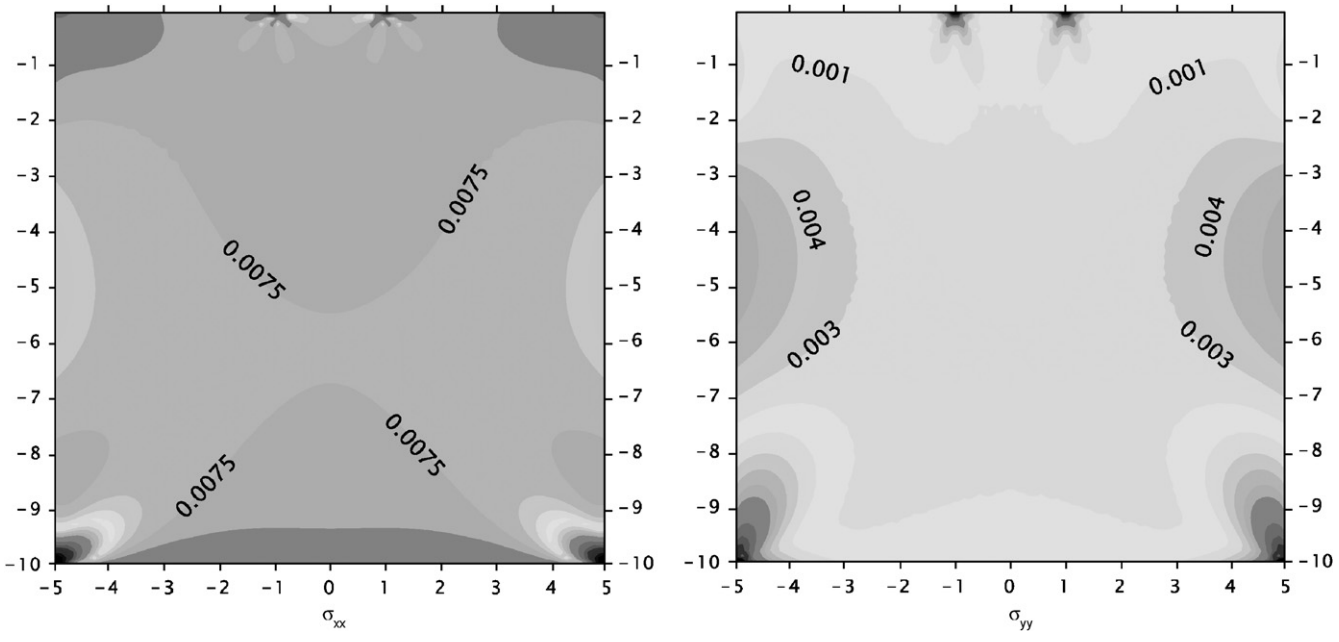

Fig. 10. Absolute error on the stress field in the core region (color levels as in Fig. 8).

Fig. 9 represents the absolute error in stress within the core region due to mesh #5 with const/log decaying infinite elements.

Comparisons in terms of accuracy are shown in Table 7 that again refers to mesh #5. The reciprocal decaying boundary element reveals to be not much accurate in

Please cite this article as: Salvadori A. Infinite boundary elements in 2D elasticity. Eng Anal Bound Elem (2007), doi:10.1016/j.enganabound.2007.06.007

evaluating the σ_{xx} component of the stress tensor. This evidence might be related to the incorrect behavior of the approximated solution in the far field with respect to the problem solution (14a), clearly shown in Fig. 7a. On the contrary, using a const/log element which reproduces the correct asymptotical behavior gives rise to extremely good approximations in the whole core region. This conclusion is worth noting because the use of such an element seems to be quite unusual.

6.2. Finite elements analyses

Five meshes have been considered. Four of them introduce artificial boundaries, as usual in a finite domain technique. In the last analysis infinite elements have been used. In analysis #1 a 10 m side square region has been discretized in a uniform way with four nodes square finite elements of side length 0.1 m. Null vertical displacements have been imposed along the lowest side (at $y = 10$ m), whereas a zero horizontal displacement has been imposed where the lowest side crosses the vertical symmetry axis. The vertical boundaries are assumed as traction free. In analysis #2 the same geometry is taken, though along the two vertical sides horizontal displacements are set equal to zero.

Analysis #3 makes use of the same finite elements of analysis #1, but the square region side length is doubled, keeping constant the element size. Constraints are taken as in analysis #1. Analysis #4 is based on the same geometry of analysis #3 but is constrained as in analysis #2.

In analysis #5 the half-plane discretization is made by adopting the same mesh of analysis #1 and suitably adding a set of 300 infinite elements of type CINPE4, implemented in Abaqus. These elements, according to [6], refer to the work by [18]. They belong to the mapped kind and are characterized by a decaying function of the type $1/r^2$, where r is the distance from a "pole", whose choice is not always straightforward.

FE and BE discretizations are only partially comparable: both BE and FE analysis #5 discretize a 10 m surface and use infinite elements to extend it, but while FE discretization is uniform (all the square elements have sides 10 cm long), BE discretization is graded and the loaded surface is discretized by elements 3 cm long (meshes #1 to #4).

6.3. Comparisons

A comparison between FEM analyses and the analytical solution in terms of accuracy of the stress tensor approximation at point $P = (0, 1)$ is performed in Table 8. In the FEM analysis point P is common to four elements. Stress components are evaluated at P by extrapolation on each element and are represented in columns 2 and 4. The percentage error in columns 3 and 5 refers to the mean value.

Figs. 8 and 9 show the error contours related to σ_{xx} (left) and σ_{yy} (right), obtained by BE analysis, when, respectively, polynomial infinite boundary elements and const–log infinite boundary elements are used. Fig. 10 refers to FE results in the discretized region when infinite elements are present at the boundary (mesh #5). The high level of accuracy obtained by using a const–log infinite boundary element is evident.

7. Conclusions and further developments

In the present note, infinite boundary elements have been formulated for static 2D problems and tested with a standard example whose analytical solution is known.

Within the framework of hypersingular boundary integral equations, a polynomial decaying, a reciprocal decaying, and a constant–logarithmic infinite boundary elements have been considered. The polynomial decaying formulation furnishes good results and memory saving with respect to a truncated mesh provided that a numerical parameter is suitably chosen. This drawback can be overcome by the other two formulations. A rationale is given for the use of reciprocal decaying shape functions, by comparing the 2D analytical solution for a strip load with the 3D Boussinesque's solution for a rectangular load when one side of the rectangle tends to infinity.

The const–log infinite boundary element proves to be effective in enhancing the accuracy of the stress field, without incrementing the computational cost of the analysis.

Further attention deserves the symmetric Galerkin formulation of the problem: a further publication will be devoted to this topic.

Appendix A. Fundamental solutions

Point load on an elastic half-plane: The fundamental solution of Flamant and Boussinesque for displacements reads as follows—see also [37]:

$$\mathscr{F}_u(x-\xi,y)=\frac{1+\nu}{\pi E}\times\begin{bmatrix} y\dfrac{-\xi+x}{(\xi-x)^2+y^2}+(-1+2\nu)\arctan\left(\dfrac{-\xi+x}{y}\right) \\ 1-\dfrac{(\xi-x)^2}{(\xi-x)^2+y^2}+(1-\nu)\log(b^2)-(1-\nu)\log((\xi-x)^2+y^2)\end{bmatrix}. \tag{33}$$

The fundamental solution of Flamant and Boussinesque for stresses reads as follows—see also [3]-:

$$\mathscr{F}_\sigma(x-\xi,y)=\frac{-2y}{\pi((\xi-x)^2+y^2)^2}\times\begin{bmatrix}(\xi-x)^2 & (-\xi+x)y \\ (-\xi+x)y & y^2\end{bmatrix}. \tag{34}$$

Please cite this article as: Salvadori A. Infinite boundary elements in 2D elasticity. Eng Anal Bound Elem (2007), doi:10.1016/j.enganabound.2007.06.007

Point load on an elastic half-space: By defining $r \stackrel{def}{=} \sqrt{(\xi - x)^2 + (\chi - y)^2 + z^2}$, the fundamental solution of Boussinesque for displacements reads as follows—see also [3]:

$$\mathscr{B}_u(x-\xi, y-\chi, z) = \frac{\kappa}{2r}\left(2(1-\nu) + \frac{z^2}{r^2}\right). \tag{35}$$

Appendix B. Mathematica subroutines

3D analysis:

```
Variable definition
r = Sqrt [(x − xp)^2 + (y − yp)^2 + zp^2];
Uz = chi 1/r(2(1 − v) + zp^2/r^2);
Integration on the load surface
fx = Simplify[Integrate[Uz, {x, −1, 1}]];
uz = FullSimplify[Integrate[fx, {y, −b/2, b/2}],
Trig − >True];
Projection on the y = 0 plane
uzb = FullSimplify[uz/.yp−> 0, Trig −> True]
Expansion around infinity
uzb00 = FullSimplify[Series[uzb, {b, Infinity, 0}]]
```

2D analysis:

```
Variable definition
Uy = 2chi(−(x − xp)^2(x − xp)^2 + zp^2 + (−1 + v)
Log[(x − xp)^2 + zp^2] − 2(−1 + v) Log[b] + 1)
Integration on the load strip
uy = FullSimplify[Integrate[Uy, {x, −1, 1}]]
```

Comparisons:

```
FullSimplify[uzb00 − uy, Trig − >True]
```

Appendix C. Green's functions for linear elasticity

Define with $\mathbf{r} = \mathbf{x} - \mathbf{y}$ and $r = \|\mathbf{r}\|$. Moreover, let $\mathbf{n}(\mathbf{x})$ denote the outward normal at the boundary Γ at $\mathbf{x}$. Analogously, let $\mathbf{l}(\mathbf{y}$ denote the outward normal at the boundary Γ at $\mathbf{y}$. Green's function $\mathbf{G}_{pp}$ for linear elasticity reads as follows:

$$\begin{aligned}\mathbf{G}_{pp}(\mathbf{r};\mathbf{n}(\mathbf{x});\mathbf{l}(\mathbf{y})) &= \frac{G}{\pi}\frac{1}{r^2}\left[\mathbf{SYM}(\mathbf{r}\otimes\mathbf{n})\frac{\mathbf{r}\cdot\mathbf{l}}{r^2} + \mathbf{SYM}(\mathbf{r}\otimes\mathbf{l})\frac{\mathbf{r}\cdot\mathbf{n}}{r^2}\right] \\ &+ \frac{Gv}{\pi(1-v)}\frac{1}{r^2}\left\{\frac{\mathbf{r}\otimes\mathbf{r}}{r^2}\left[(\mathbf{l}\cdot\mathbf{n}) - \frac{4}{v}\frac{(\mathbf{r}\cdot\mathbf{n})(\mathbf{r}\cdot\mathbf{l})}{r^2}\right]\right. \\ &\left. + \left[\frac{(\mathbf{r}\cdot\mathbf{n})(\mathbf{r}\cdot\mathbf{l})}{r^2} + \frac{(1-2v)}{2v}(\mathbf{l}\cdot\mathbf{n})\right]\mathbf{I} + \mathbf{SYM}(\mathbf{l}\otimes\mathbf{n})\right\}.\end{aligned}$$

For the 2D plane stress case, one needs to substitute v with $v^* = \frac{v}{1+v}$.

Appendix D. Basic Lebesgue integrals

The following identities, that can be easily proved when $x_2 \neq 0$, are the keynote of the inner integration:

$$\int_{x_1-l^*}^{x_1+l^*} \frac{1}{r^2}\frac{1}{z_1 - r_1}\,\mathrm{d}r_1\Big|_{r_2=x_2} = \left[\frac{z_1 \arctan\left(\frac{r_1}{x_2}\right)}{x_2(x_2^2+z_1^2)} + \frac{\log\left(\frac{r_1^2+x_2^2}{(r_1-z_1)^2}\right)}{2(x_2^2+z_1^2)}\right]_{r_1=x_1-l^*}^{r_1=x_1+l^*},$$

$$\int_{x_1-l^*}^{x_1+l^*} \frac{1}{r^4}\frac{1}{z_1 - r_1}\,\mathrm{d}r_1\Big|_{r_2=x_2} = \left[\frac{-x_2^2 + r_1 z_1}{2x_2^2(r_1^2+x_2^2)(x_2^2+z_1^2)} + \frac{(3x_2^2 z_1 + z1^3)\arctan\left(\frac{r_1}{x_2}\right)}{2x_2^3(x_2^2+z_1^2)^2} + \frac{\log\left(\frac{r_1^2+x_2^2}{(r_1-z_1)^2}\right)}{2(x_2^2+z_1^2)^2}\right]_{r_1=x_1-l^*}^{r_1=x_1+l^*},$$

$$\int_{x_1-l^*}^{x_1+l^*} \frac{1}{r^4}\frac{r_1}{z_1 - r_1}\,\mathrm{d}r_1\Big|_{r_2=x_2} = \left[\frac{-r_1 - z_1}{2(r_1^2+x_2^2)(x_2^2+z_1^2)} + \frac{(-x_2^2+z_1^2)\arctan\left(\frac{r_1}{x_2}\right)}{2x_2(x_2^2+z_1^2)^2} + \frac{z_1 \log\left(\frac{r_1^2+x_2^2}{(r_1-z_1)^2}\right)}{2(x_2^2+z_1^2)^2}\right]_{r_1=x_1-l^*}^{r_1=x_1+l^*},$$

$$\int_{x_1-l^*}^{x_1+l^*} \frac{1}{r^4}\frac{r_1^2}{z_1 - r_1}\,\mathrm{d}r_1\Big|_{r_2=x_2} = \left[\frac{x_2^2 - r_1 z_1}{2(r_1^2+x_2^2)(x_2^2+z_1^2)} + \frac{(-(x_2^2 z_1) + z_1^3)\arctan\left(\frac{r_1}{x_2}\right)}{2x_2(x_2^2+z_1^2)^2} + \frac{z_1^2 \log\left(\frac{r_1^2+x_2^2}{(r_1-z_1)^2}\right)}{2(x_2^2+z_1^2)^2}\right]_{r_1=x_1-l^*}^{r_1=x_1+l^*},$$

$$\int_{x_1-l^*}^{x_1+l^*} \frac{1}{r^6}\frac{1}{z_1 - r_1}\,\mathrm{d}r_1\Big|_{r_2=x_2} = \left[\frac{-x_2^2 + r_1 z_1}{4x_2^2(r_1^2+x_2^2)^2(x_2^2+z_1^2)} + \frac{-4x_2^4 + 7r_1 x_2^2 z_1 + 3r_1 z_1^3}{8x_2^4(r_1^2+x_2^2)(x_2^2+z_1^2)^2} + \frac{(15x_2^4 z_1 + 10x_2^2 z_1^3 + 3z_1^5)\arctan\left(\frac{r_1}{x_2}\right)}{8x_2^5(x_2^2+z_1^2)^3} + \frac{\log\left(\frac{r_1^2+x_2^2}{(r_1-z_1)^2}\right)}{2(x_2^2+z_1^2)^3}\right]_{r_1=x_1-l^*}^{r_1=x_1+l^*},$$

Please cite this article as: Salvadori A. Infinite boundary elements in 2D elasticity. Eng Anal Bound Elem (2007), doi:10.1016/j.enganabound.2007.06.007

$$\int_{x_1-l^*}^{x_1+l^*} \frac{1}{r^6}\frac{r_1}{z_1-r_1}\,\mathrm{d}r_1\bigg|_{r_2=x_2} = \left[\frac{-r_1-z_1}{4(r_1^2+x_2^2)^2(x_2^2+z_1^2)} + \frac{-3r_1x_2^2-4x_2^2z_1+r_1z_1^2}{8x_2^2(r_1^2+x_2^2)(x_2^2+z_1^2)^2} + \frac{(-3x_2^4+6x_2^2z_1^2+z_1^4)\arctan\left(\frac{r_1}{x_2}\right)}{8x_2^3(x_2^2+z_1^2)^3} + \frac{z_1\log\left(\frac{r_1^2+x_2^2}{(r_1-z_1)^2}\right)}{2(x_2^2+z_1^2)^3}\right]_{r_1=x_1-l^*}^{r_1=x_1+l^*},$$

$$\int_{x_1-l^*}^{x_1+l^*} \frac{1}{r^6}\frac{r_1^2}{z_1-r_1}\,\mathrm{d}r_1\bigg|_{r_2=x_2} = \left[\frac{x_2^2-r_1z_1}{4(r_1^2+x_2^2)^2(x_2^2+z_1^2)} + \frac{-3r_1x_2^2z_1-4x_2^2z_1^2+r_1z_1^3}{8x_2^2(r_1^2+x_2^2)(x_2^2+z_1^2)^2} + \frac{(-3x_2^4z_1+6x_2^2z_1^3+z_1^5)\arctan\left(\frac{r_1}{x_2}\right)}{8x_2^3(x_2^2+z_1^2)^3} + \frac{z_1^2\log\left(\frac{r_1^2+x_2^2}{(r_1-z_1)^2}\right)}{2(x_2^2+z_1^2)^3}\right]_{r_1=x_1-l^*}^{r_1=x_1+l^*},$$

$$\int_{x_1-l^*}^{x_1+l^*} \frac{1}{r^6}\frac{r_1^3}{z_1-r_1}\,\mathrm{d}r_1\bigg|_{r_2=x_2} = \left[\frac{r_1x_2^2+x_2^2z_1}{4(r_1^2+x_2^2)^2(x_2^2+z_1^2)} + \frac{-(r_1x_2^2)-5r_1z_1^2-4z_1^3}{8(r_1^2+x_2^2)(x_2^2+z_1^2)^2} + \frac{(-x_2^4-6x_2^2z_1^2+3z_1^4)\arctan\left(\frac{r_1}{x_2}\right)}{8x_2(x_2^2+z_1^2)^3} + \frac{z_1^3\log\left(\frac{r_1^2+x_2^2}{(r_1-z_1)^2}\right)}{2(x_2^2+z_1^2)^3}\right]_{r_1=x_1-l^*}^{r_1=x_1+l^*}.$$

Appendix E. Tables

In this appendix, tables $\mathbf{L}_{pp}$, $\mathbf{A}_{pp}$, $\mathbf{S}_{pp}$, $\mathbf{H}_{pp}$ are collected.

$$\kappa_{log} = \frac{G}{4\pi(-1+\nu)(x_2^2+z_1^2)^3},$$

$$\mathbf{L}_{pp}[1,1] = \kappa_{log}(-n_2x_2^4 - 2n_1x_2^3z_1 + 6n_2x_2^2z_1^2 + 6n_1x_2z_1^3 - n_2z_1^4),$$

$$\mathbf{L}_{pp}[1,2] = \kappa_{log}(-n_1x_2^4 + 6n_2x_2^3z_1 + 6n_1x_2^2z_1^2 - 2n_2x_2z_1^3 - n_1z_1^4) = \mathbf{L}_{pp}[2,1],$$

$$\mathbf{L}_{pp}[2,2] = \kappa_{log}(3n_2x_2^4 + 6n_1x_2^3z_1 - 6n_2x_2^2z_1^2 - 2n_1x_2z_1^3 - n_2z_1^4),$$

$$\kappa_{arc} = \frac{G}{\pi(-1+\nu)(x_2^2+z_1^2)^3},$$

$$\mathbf{A}_{pp}[1,1] = \kappa_{arc}(-2n_2x_2^3z_1 - 3n_1x_2^2z_1^2 + 2n_2x_2z_1^3 + n_1z_1^4),$$

$$\mathbf{A}_{pp}[1,2] = \kappa_{arc}(-n_2x_2^4 - 2n_1x_2^3z_1 + 3n_2x_2^2z_1^2 + 2n_1x_2z_1^3) = \mathbf{A}_{pp}[2,1],$$

$$\mathbf{A}_{pp}[2,2] = \kappa_{arc}(-n_1x_2^4 + 4n_2x_2^3z_1 + 3n_1x_2^2z_1^2),$$

$$\kappa_S = \kappa_H = \frac{G}{2\pi(-1+\nu)(x_2^2+z_1^2)^2},$$

$$\mathbf{S}_{pp}[1,1] = \kappa_S(x_2^2(-3n_2r_1+n_1x_2)z_1 - 4x_2(n_1r_1+n_2x_2)z_1^2 - (-n_2r_1+3n_1x_2)z_1^3),$$

$$\mathbf{S}_{pp}[1,2] = \kappa_S(-2n_2r_1x_2^3 - 3x_2^2(n_1r_1+n_2x_2)z_1 - 2x_2(-n_2r_1+2n_1x_2)z_1^2 + (n_1r_1+n_2x_2)z_1^3) = \mathbf{S}_{pp}[2,1],$$

$$\mathbf{S}_{pp}[2,2] = \kappa_S(-2x_2^3(n_1r_1+n_2x_2) - x_2^2(-5n_2r_1+3n_1x_2)z_1 + 2x_2(n_1r_1+n_2x_2)z_1^2 + (n_2r_1+n_1x_2)z_1^3),$$

$$\mathbf{H}_{pp}[1,1] = \kappa_H(2x_2^5(n_1r_1+n_2x_2) + 2x_2^4(-n_2r_1+n_1x_2)z_1 + 2x_2^3(n_1r_1+n_2x_2)z_1^2 + 2x_2^2(-n_2r_1+n_1x_2)z_1^3),$$

$$\mathbf{H}_{pp}[1,2] = \kappa_H(2x_2^5(-n_2r_1+n_1x_2) - 2x_2^4(n_1r_1+n_2x_2)z_1 - 2x_2^3(-n_2r_1+n_1x_2)z_1^2 - 2x_2^2(n_1r_1+n_2x_2)z_1^3) = \mathbf{H}_{pp}[2,1],$$

$$\mathbf{H}_{pp}[2,2] = \kappa_H(-2x_2^5(n_1r_1+n_2x_2) - 2x_2^4(-n_2r_1+n_1x_2)z_1 - 2x_2^3(n_1r_1+n_2x_2)z_1^2 - 2x_2^2(-n_2r_1+n_1x_2)z_1^3),$$

References

[1] Geers TL. Computational methods for unbounded domains. Dordrecht: Kluwer Academic Publishers; 1998.
[2] Givoli D. Numerical methods for problems in infinite domains. Amsterdam: Elsevier; 1992.
[3] Bettess P. Infinite elements. UK: Penshaw Press; 1992.
[4] Zerfa FZ, Loret B. Coupled dynamic elasticplastic analysis of earth structures. Soil Dyn Earthq Eng 2003;23:435–54.
[5] Lysmer J, Kuhlemeyer RL. Finite dynamic model for infinite media. J Eng Mech Div ASCE 1969;95:859–77.
[6] Hibbitt, Karlsson, Sorensen. ABAQUS/standard theory manual, vol. 6(4), 2004.
[7] Telles JCF, Brebbia CA. Boundary element solution for half-plane problems. Int J Solids Struct 1981;17:1149–58.
[8] Pan L, Rizzo F, Martin PA. Some efficient boundary integral strategies for time-harmonic wave problems in an elastic halfspace. Comput Methods Appl Mech Eng 1998;164:207–21.
[9] Apsel RJ, Luco JE. Impedance functions for foundations embedded in a layered medium: an integral equation approach. Earthq Eng Struct Dyn 1987;15:213–31.

Please cite this article as: Salvadori A. Infinite boundary elements in 2D elasticity. Eng Anal Bound Elem (2007), doi:10.1016/j.enganabound.2007.06.007

[10] Chapel F. Boundary element method applied to linear soil structure interaction on a heterogeneous soil. Earthq Eng Struct Dyn 1987;15:815–29.
[11] Liang J, Liew KM. Boundary elements for half-space problems via fundamental solutions: a three-dimensional analysis. Int J Numer Methods Eng 2001;52:1189–202.
[12] Dominguez J, Roesset JM. Dynamic stiffness of rectangular foundations. Technical Report, MIT Research Report R 78-20, 1978.
[13] Abdel-Fattah TT, Hodhod HA, Akl AY. A novel formulation of infinite elements for static analysis. Comput Struct 2000;77:371–9.
[14] Ungless RF. An infinite finite element. Master's thesis, University of British Columbia, 1973.
[15] Bettess P. Infinite elements. Int J Numer Methods Eng 1977;12:53–64.
[16] Bettess P. More on infinite elements. Int J Numer Methods Eng 1980;15:1613–26.
[17] Beer G, Meek JL. Infinite-domain elements. Int J Numer Methods Eng 1981;17:43–52.
[18] Zienkiewicz OC, Emson C, Bettess P. A novel boundary infinite element. Int J Numer Methods Eng 1983;19:393–404.
[19] Watson JO. Advanced implementation of the boundary element method for two and three dimensional elastostatics. In: Banerjee PK, Butterfield R, editors. Developments in boundary element methods—I. Elsevier Applied Science Publishers; 1979. p. 31–63.
[20] Beer G, Watson JO. Infinite boundary elements. Int J Numer Methods Eng 1989;28:1233–47.
[21] Davies TG, Bu S. Infinite boundary elements for the analysis of halfspace problems. Comput Geotech 1996;19(2):137–51.
[22] Gao XW, Davies TG. 3d infinite boundary elements for half space problems. Eng Anal Boundary Elem 1998;21:207–13.
[23] Johnson KL. Contact mechanics. Cambridge: Cambridge University Press; 1985.
[24] El-Esnawy NA, Akl AY, Bazaraa AS. A new parametric infinite domain element. Finite Elem Anal Des 1995;19:103–14.
[25] Cheng YM. The use of infinite element. Comput Geotechn 1996;18:65–70.
[26] Koh KH, Lee SR. p-version static infinite element for representing $1/r^n$ type decay problems in unbounded media. Comput Geotehn 1998;22(1):73–89.
[27] Kumar P. Finite element method computations in unbounded domains with nonzero but uniform far field decay. Comput Struct 2000;75(7):457–62.
[28] Kumar P. Infinite elements for numerical analysis of underground excavations. Tunnelling Underground Space Technol 2000;15(1):117–24.
[29] Bonnet M, Maier G, Polizzotto C. Symmetric Galerkin boundary element method. Appl Mech Rev 1998;51:669–704.
[30] Salvadori A. Analytical integrations in 2D BEM elasticity. Int J Numer Methods Eng 2002;53(7):1695–719.
[31] Monegato G, Scuderi L. Numerical integration of functions with boundary singularities. J Comput Appl Math 1999;112:201–14.
[32] Mantič V. On computing boundary limiting values of boundary integrals with strongly singular and hypersingular kernels in 3d bem for elastostatics. Eng Anal Boundary Elem 1994;13:115–34.
[33] Hong KH, Chen JT. Derivations of integral equations of elasticity. ASCE J Eng Mech 1988;114(6):1028–44.
[34] McLean W. Strongly elliptic systems and boundary integral equations. New York: Cambridge University Press; 2000.
[35] Holzer S. How to deal with hypersingular integrals in the symmetric BEM. Commun Appl Numer Methods 1993;9:219–32.
[36] Gray LJ, Martha LF, Ingraffea AR. Hypersingular integrals in boundary element fracture analysis. Int J Numer Methods Eng 1990;29:1135–58.
[37] Baldacci R. Scienza delle costruzioni, vol. I. UTET, 1970 [in Italian].
[38] Corradi Dell'Acqua L. Meccanica delle strutture, vol. I. Milano: Mc Graw Hill, 1992 [in Italian].
[39] Brebbia CA, Telles JCF, Wrobel LC. Boundary element techniques. Berlin: Springer; 1984.
[40] Deeks AJ, Wolf JP. Semi-analytical elastostatic analysis of unbounded two-dimensional domains. Int J Numer Anal Methods Geomech 2002;26:1031–57.
[41] Zemanian AH. Distribution theory and transform analysis. New York: Dover; 1987.
[42] Salvadori A. Hypersingular boundary integral equations and the approximation of the stress tensor, Int J Numer Methods Eng 2006, in press, doi:10.1002/nme.2041.

Please cite this article as: Salvadori A. Infinite boundary elements in 2D elasticity. Eng Anal Bound Elem (2007), doi:10.1016/j.enganabound.2007.06.007